https://doi.org/10.5194/acp-2020-84
Preprint. Discussion started: 4 March 2020
© Author(s) 2020. CC BY 4.0 License.

Atmospheric Chemistry and Physics Discussions

Molecular Insights into New Particle Formation in Barcelona, Spain

James Brean[1], David C.S. Beddows[1], Zongbo Shi[1], Brice Temime-Roussel[2], Nicolas Marchand[2], Xavier Querol[3], Andrés Alastuey[3], María Cruz Minguillón[3], and Roy M. Harrison[1a*]

[1]Division of Environmental Health and Risk Management School of Geography, Earth and Environmental Sciences University of Birmingham, Edgbaston, Birmingham B15 2TT United Kingdom

[2]Aix Marseille Univ, CNRS, LCE Marseille, 13003, France

[3]Institute of Environmental Assessment and Water Research (IDAEA-CSIC), Barcelona, 08034 Spain

[a]Also at: Department of Environmental Sciences / Center of Excellence in Environmental Studies, King Abdulaziz University, PO Box 80203, Jeddah, 21589, Saudi Arabia

[*] To whom correspondence should be addressed (Email: r.m.harrison@bham.ac.uk)

https://doi.org/10.5194/acp-2020-84
Preprint. Discussion started: 4 March 2020
© Author(s) 2020. CC BY 4.0 License.

Atmospheric Chemistry and Physics Discussions

ABSTRACT

Atmospheric aerosols contribute some of the greatest uncertainties to estimates of global radiative forcing, and have significant effects on human health. New particle formation (NPF) is the process by which new aerosols of sub-2 nm diameter form from gas-phase precursors and contributes significantly to particle numbers in the atmosphere, accounting for approximately 50% of cloud condensation nuclei globally. Here, we study summertime NPF in urban Barcelona in NE Spain. The rate of formation of new particles is seen to increase linearly with sulphuric acid concentration in a manner similar to systems studied in chamber studies involving sulphuric acid, water and dimethylamine (DMA), as well as sulphuric acid, water and the oxidation products of pinanediol. The sulphuric acid dimer:monomer ratio is significantly lower than that seen in experiments involving sulphuric acid and DMA in chambers, indicating that stabilization of sulphuric acid clusters by bases is weaker in this dataset than in chambers, and thus another mechanism, likely involving the plentiful highly oxygenated organic molecules (HOMs) is plausible. The high concentrations of HOMs arise largely from both alkylbenzene and monoterpene oxidation, with the former providing greater concentrations of HOMs due to significant local sources. The concentration of these HOMs shows a dependence on both temperature and precursor VOC concentration. New particle formation without growth past 10 nm is also observed, and on these days the highly oxygenated organic compound concentration is significantly lower than on days with growth, and thus high concentrations of low volatility oxygenated organics appear to be a necessary condition for the growth of newly formed particles in Barcelona. These results are consistent with prior observations of new particle formation in both chambers and the real atmosphere, and these results are likely representative of the urban background of many European Mediterranean cities.

https://doi.org/10.5194/acp-2020-84
Preprint. Discussion started: 4 March 2020
© Author(s) 2020. CC BY 4.0 License.

Atmospheric Chemistry and Physics Discussions

1. INTRODUCTION

Atmospheric aerosols, defined as liquid or solid droplets suspended in a gas, affect the climate both directly by scattering and absorbing radiation, and indirectly by acting as cloud condensation nuclei (CCN) (Penner et al., 2011), providing great uncertainties in estimates of global radiative forcing (IPCC, 2014). Further, fine ambient aerosols (defined as those with diameter below 2.5 μm) are the fifth greatest global mortality risk factor, resulting in 103.1 million disability-adjusted life year loss in 2015 (Cohen et al., 2017). The number concentration of the ultrafine fraction of these (aerosols with diameter below 0.1 μm, referred to as ultrafine particles or UFP) pose potentially significant health risks also, due to their high concentration and surface area. The more diffuse, gas-like behaviour of UFP allows them to penetrate into the deep lung and enter the bloodstream (Miller et al., 2017). Ultrafine particles occur in the urban environment either as primary emissions (i.e., from car exhaust (Harrison et al., 2018)) or secondarily as the product of new particle formation (NPF) (Agudelo-Castañeda et al., 2019; Bousiotis et al., 2019)

NPF is the formation of aerosol particles from gas-phase precursors. NPF can be considered a two-step process involving initial formation of a cluster of gas molecules at the critical diameter at around 1.5 nm - the diameter at which a free-energy barrier must be overcome to allow the spontaneous phase transition from gas to liquid or solid (Zhang et al., 2012), and the subsequent growth of this droplet to a larger aerosol particle. The first step of this process is dependent upon the stability and abundance of the clustering molecules. Sulphuric acid, water, and dimethylamine (DMA), for example, efficiently form particles as the strong hydrogen bonding between the acid base pair produces near negligible evaporation, much lower than the evaporation rate seen for the more weakly bound sulphuric acid-ammonia-water system. Nucleation of sulphuric acid, DMA and water proceeds at, or near to the kinetic limit (Almeida et al., 2013; Kurtén et al., 2008). Once past this 1.5 nm diameter, condensation and coagulation will drive particle growth. Both the abundance of condensable gases and their vapour pressures limit condensational growth. Vapour pressures are

https://doi.org/10.5194/acp-2020-84
Preprint. Discussion started: 4 March 2020
© Author(s) 2020. CC BY 4.0 License.

Atmospheric Chemistry and Physics Discussions

77 especially important for the initial growth stages, as the Kelvin effect barrier impairs condensation
78 of more volatile species, with this condition of low vapour pressures becoming less significant as
79 the diameter of the particle increases (Tröstl et al., 2016). Once sufficiently large (>50 nm), the loss
80 processes for these particles become inefficient, resulting in a significant atmospheric lifetime. It is
81 at these diameters the climate forcing effects of these particles become most pronounced.
82
83 NPF processes happen globally, across a diverse range of environments from pristine polar regions,
84 to polluted urban megacities (Kerminen et al., 2018), and represent a significant source of CCN,
85 with 10-60% of NPF events shown to produce CCN and enhancement factors to CCN count ranging
86 from 0.5 – 1.1 (Lee et al., 2019 and references within). Strong NPF events are observed across a
87 range of urban environments, despite high condensation sinks (Bousiotis et al., 2019; Yu et al.,
88 2016), and can act as a precursor to strong haze events (Guo et al., 2014). Urban NPF occurs despite
89 extremely high condensation sinks, an effect which has only been partially explained by growing
90 understanding from recent in-depth studies (Yao et al., 2018). Recent advances in instrumentation
91 allow for the measurement of particles down to the critical diameter with instruments such as the
92 particle size magnifier (PSM), and (Neutral) Air Ion Spectrometer (NAIS/AIS) (Lee et al., 2019),
93 and mass spectral techniques for measuring the abundance and composition of neutral (Jokinen et
94 al., 2012) and charged (Junninen et al., 2010) clusters. Elucidated mechanisms with these
95 techniques involve sulphuric acid and ammonia in remote environments (Jokinen et al., 2018; Yan,
96 2018), monoterpene derived highly oxygenated molecules (HOM) in remote environments (Rose et
97 al., 2018), iodic acid in coastal environments (Sipilä et al., 2016), and sulphuric acid and DMA in
98 polluted urban environments (Yao et al., 2018).
99
100 Urban Barcelona sees frequent, strong summer-time NPF events. These events are associated with
101 high insolation and relatively high ozone when considering the whole year (Brines et al., 2014,
102 2015). This has been also reported in other urban environments such as Los Angeles, Brisbane,

https://doi.org/10.5194/acp-2020-84
Preprint. Discussion started: 4 March 2020
© Author(s) 2020. CC BY 4.0 License.

Rome and Madrid (Brines et al., 2015). However, when considering mid-summer, maximum ozone episodes are typically associated with high aerosol load, but not with NPF around the regional background of Barcelona (Carnerero et al., 2019; Querol et al., 2017). Ground-level observations report NPF events starting typically at midday, and either occurring in urban Barcelona and the surrounding regional background simultaneously, or isolated to just urban Barcelona, or just the regional background (Dall'Osto et al., 2013). Vertical profiles over urban Barcelona reveal that NPF occurs at higher altitudes, and starts earlier in the day, as at a given altitude these events are not suppressed by early traffic peaks contributing to particle load (Minguillón et al., 2015). Here, we examine molecular level evidence for formation of particles at the critical diameter from sulphuric acid in Barcelona, with possible contribution from strong bases and highly oxygenated organic molecules (HOMs), as well as factors influencing subsequent particle growth.

2. METHODS

2.1 Sampling Site

The Palau Reial site in Barcelona (41°23'15" N, 2°6'53.64" E) is representative of the urban background of Barcelona, located at the Institute of Environmental Assessment and Water Research (IDAEA-CSIC) in the north-west of the city. Sampling was performed from a container 20 m from a low traffic road, and 200 m from the nearest main road (Avinguda Diagonal). Data were taken from 2018/06/28 through 2018/07/18.

2.2 Chemical Ionisation Atmospheric Pressure Interface Time of Flight Mass Spectrometry

The Aerodyne Nitrate Chemical Ionisation Atmospheric Pressure Interface Time of Flight Mass Spectrometer (CI-APi-ToF) was used to make measurements of neutral oxygenated organic compounds, organic and inorganic acids, bases, and their molecular clusters at high time resolution with high resolving power. The ionization system charges molecules by adduct formation, such as

https://doi.org/10.5194/acp-2020-84
Preprint. Discussion started: 4 March 2020
© Author(s) 2020. CC BY 4.0 License.

Atmospheric Chemistry and Physics Discussions

in the case of organic compounds with two or more hydrogen bond donor groups (Hyttinen et al., 2015), or proton transfer in the case of strong acids like sulphuric acid (Jokinen et al., 2012). Hydroxyl or hydroperoxyl functionalities are both common hydrogen bond donating groups, with hydroperoxyl being the more efficient hydrogen bond donor (Møller et al., 2017). This instrument has been explained in great detail elsewhere (Jokinen et al., 2012; Junninen et al., 2010), but briefly, the front end consists of a chemical ionisation system where a 10 L min^{-1} sample flow is drawn in through the 1 m length 1" OD stainless steel tubing opening. A secondary flow was run parallel and concentric to this sample flow, rendering the reaction chamber effectively wall-less. A 3 cm^3 min^{-1} flow of a carrier gas (N_2) is passed over a reservoir of liquid HNO_3, entraining vapour which is subsequently ionised to NO_3^- via an X-ray source. This flow is then guided into the sample flow. The nitrate ions will then charge molecules either by clustering or proton transfer. The mixed flows travelling at 10 L min^{-1} enter the critical orifice at the front end of the instrument at 0.8 L min^{-1} and are guided through a series of differentially pumped chambers before reaching the ToF analyser. All data analysis was carried out in the Tofware package in Igor Pro 7 (Tofwerk AG, Switzerland). Sensitivity of 3×10^9 cm^{-3} was assumed based upon a prior calibration (Brean et al., 2019) and comparison with a calculated sulphuric acid proxy (Mikkonen et al., 2011). Due to the high resolving power of the CI-APi-ToF system (mass resolving power of 3000, and mass accuracy of 20 ppm at 201 m/Q), multiple peaks can be fit at the same unit mass and their molecular formulae assigned. Beyond 500 m/Q, peak fitting and assignment of compositions becomes problematic as signal decreases, mass accuracy decreases, and the total number of possible chemical compositions increases, so peaks above the C_{20} region have not been assigned (Cubison and Jimenez, 2015), however, signals past this region tended to be extremely low. As proton transfer mostly happens with acids, and nearly all HOM molecules will be charged by adduct formation it is possible to infer the uncharged formula; therefore, all HOMs from here onwards will be listed as their uncharged form. The CI-APi-ToF inlet was placed approximately 1.5 m a.g.l. CI-APi-ToF data is only available between the dates 2018/07/06 and 2018/07/17.

https://doi.org/10.5194/acp-2020-84
Preprint. Discussion started: 4 March 2020
© Author(s) 2020. CC BY 4.0 License.

Atmospheric Chemistry and Physics Discussions

2.2 Particle Size and Number Measurements

Two Scanning Mobility Particle Sizer (SMPS) instruments measured particle size distributions at 5 minute time resolution, one Long Column SMPS (TSI 3080 EC, 3082 Long DMA, 3772 CPC, TSI, USA) and one NanoSMPS (3082 EC, 3082 Nano DMA, 3776 CPC, TSI, USA) measuring the ranges 10.9 – 478.3 nm and 4.5 – 65.3 nm respectively. A Particle Size Magnifier (A10, Airmodus, FN) linked to a CPC (3775, TSI, USA) measured the sub-3 nm size fraction. The PSM was run in stepping mode, operating at four different saturator flows to vary the lower size cut of particles that it will grow (defined as the point of 50% efficiency, D_{50}). This was set at 4 flows giving D_{50} from 1.4 to 2.4 nm. The instrument switched between saturator flows each 2.5 minutes, giving a sub-2.4 nm size distribution every 10 minutes. Aerosol sampling inlets were placed approximately 2 m a.g.l.

2.3 Other Measurements

Mixing ratios of non-methane VOC with proton affinity greater than H_3O^+ were made using the proton transfer reaction time of flight mass spectrometer (PTR-ToF-MS 8000, Ionicon Analytik GmbH, Austria). A detailed description of the instrument is provided by Graus et al., (2010) The sampling set up, operating conditions, and quantification procedures are similar to those described in Minguillón et al. (2016). Continual monitoring of composition and mass of submicron aerosol was carried out with an Aerosol Chemical Speciation Monitor (ACSM, Aerodyne, USA) (Ng et al., 2011). Ozone, NO, and NO_2 were measured by conventional ultraviolet and chemiluminiscence air quality instrumentation. Meteorological data were supplied by the Faculty of Physics of University of Barcelona, from a nearby (200 m from the measurement site) meteorological station located at the roof of an 8 floor building.

2.4 Condensation Sink and Particle Growth Rate

The condensation sink (CS) represents the rate at which a vapour phase molecule will collide with pre-existing particle surface, and was calculated from the size distribution data as follows:

https://doi.org/10.5194/acp-2020-84
Preprint. Discussion started: 4 March 2020
© Author(s) 2020. CC BY 4.0 License.

Atmospheric Chemistry and Physics Discussions

$$CS = 4\pi D \sum_{d_p} \beta_{m,d_p} d_p N_{d_p} , \quad (1)$$

where D is the diffusion coefficient of the diffusing vapour (assumed sulphuric acid), β_m is a transition regime correction (Kulmala et al., 2001), d_p is particle diameter, and N_{dp} is the number of particles at diameter d_p. The formation rate of new particles at size d_p is calculated as follows:

$$J_{d_p} = \frac{dN_{d_p}}{dt} + CoagS_{d_p} . N_{d_p} + \frac{GR}{\Delta d_p} . N_{d_p} \quad (2)$$

Where the first term on the right-hand side comprises the rate at which particles enter the size d_p, and the latter two terms represent losses from this size by coagulation and growth respectively. See Kulmala et al. (2001) for more information on calculation of coagulation sinks and formation rates, and Kulmala et al. (2012) for calculation of growth rates.

3. RESULTS AND DISCUSSION

3.1 General Conditions of NPF Events

Summer NPF events in the regional background around Barcelona are associated with high insolation, relatively low ozone (high compared with the rest of the year), and lower particulate matter load (Brines et al., 2014; Carnerero et al., 2019). Figure 1 shows an example of a day with no NPF in panel (a), referred to as “non-event” here, where two traffic-associated peaks in particle number are seen during rush hours. Midday traffic peaks are also seen on certain days, but these are easily distinguished from nucleation processes due to the lack of a significant <10 nm mode. Figure 1(b) shows a nucleation day with growth to larger sizes >10 nm, termed “full-event”, showing the growth through the course of the day. These fulfil all the criteria of Dal Maso et al. (2005). Figure 1(c) shows a day with nucleation occurring, but no growth past 10 nm. These days are referred to as “burst-event” days. Here, NPF is seen to occur, but particles fail to grow past the nucleation mode. Two such events were seen in this data, and both are accompanied by a distinct mode appearing beforehand at ~20-40 nm. Condensation sinks were not significantly higher than on full event days, so this failure of particles to grow further cannot be attributed to condensational losses.

https://doi.org/10.5194/acp-2020-84
Preprint. Discussion started: 4 March 2020
© Author(s) 2020. CC BY 4.0 License.

Atmospheric Chemistry and Physics Discussions

207

208 Figure 2 contains box plots showing condensation sink, temperature and global radiation for all 3
209 NPF types. Condensation sinks during NPF periods of both types (Figure 1(b) & 1(c)) were not
210 significantly lower than in non-event periods. Global radiation and temperature were higher for full-
211 event, most significantly for temperature. Figure 3 is as Figure 2 but for sulphuric acid, ammonia
212 and amines, and HOMs as measured by CI-APi-ToF. Sulphuric acid is elevated during both full-
213 event and burst-event periods. In urban Barcelona, sulphuric acid will primarily arise from
214 oxidation of SO_2 by the $OH^{\cdot}$ radical, with anthropogenic emissions such as shipping emissions from
215 the port areas being significant sources of SO_2 (Henschel et al., 2013). Direct traffic emissions have
216 been shown to be a significant primary sulphuric acid source (Olin et al., 2020), but our sulphuric
217 acid data show no traffic peaks. Ammonia and amines show enhancement for full-event periods, but
218 not burst-event periods. Nucleation rates (at typical tropospheric sulphuric acid concentrations) are
219 sensitive to amine concentrations in the range of a few pptv, with enhancements to amine mixing
220 ratios past this point increasing the nucleation rate marginally (Almeida et al., 2013).
221 Concentrations of DMA and other alkylamines vary from zero to a few pptv in the boundary layer.

222

223 Barcelona has been shown to contain ppbv levels of ammonia (Pandolfi et al., 2012), arising from
224 both agriculture to the north (Van Damme et al., 2018), and anthropogenic activities such as waste
225 management and traffic, with waste management being the primary ammonia source. Highest
226 ammonia mixing ratios are found in the densely populated old city centre (Reche et al., 2015).
227 Agriculture, waste management, and traffic are also all significant sources of low molecular weight
228 alkylamines, such as DMA (Ábalos et al., 1999; Cadle and Mulawa, 1980; Hutchinson et al., 1982;
229 Ge et al., 2011), and are likely the source of amines found in this dataset. Activities such as
230 composting and food industry are especially strong sources of trimethylamine (TMA) (Ge et al.,
231 2011). A similar tertiary amine, trimethylamine (TEA) has been shown to be highly inefficient at
232 forming particles with sulphuric acid, likely due to its inability to form strong hydrogen bonded

https://doi.org/10.5194/acp-2020-84
Preprint. Discussion started: 4 March 2020
© Author(s) 2020. CC BY 4.0 License.

Atmospheric Chemistry and Physics Discussions

pairs (Glasoe et al., 2015), and NO_3^- ionization is therefore likely not sensitive to tertiary amines. As the charging mechanism of amines is similar to the mechanism by which amines form clusters with sulphuric acid, the sensitivities will be roughly similar to the strength of the bonding within sulphuric acid clusters, therefore, although significant levels of TMA are expected, they were not seen in the CI-APi-ToF spectra, nor will they participate efficiently in nucleation. The quantification of amines seen in the CI-APi-ToF is highly uncertain, with sensitivities likely being dependent upon the efficiency with which an amine will form a cluster with the nitrate trimer in the CI-APi-ToF, so no mixing ratios have been calculated from these signals (Simon et al., 2016). All ammonia and amine signals follow similar trends, indicating similar sources (R^2 ranging from 0.34 – 0.89 between ammonia and amines). The relative strength of these signals are shown in Figure S1, with significantly higher signals attributed to ammonia compared to amines, despite a likely lower sensitivity (Simon et al., 2016). HOM concentrations were greatly enhanced during full-event periods, but lower during burst-event periods, implying their necessity for growth. Further, all full and burst events are associated with southerly and south-westerly air masses. Despite this, concentrations of iodine and DMS-derived acids such as iodic acid (HIO_3) and methanesulphonic acid (MSA) are low, indicating a small influence of oceanic emissions on particle nucleation/growth.

3.2 Mechanisms of New Particle Formation

The correlation between J_5 and ion signals for sulphuric acid is plotted in Figure 4. J_5 is used here in place of $J_{1.5}$ due to better data coverage. A close relationship between NPF rates and sulphuric acid concentrations (R^2 = 0.49) are consistent with observations globally (Lee et al., 2019). This relationship is not dependent upon condensation sink. These NPF rates have no dependence on other ions as measured by CI-APi-ToF, including HIO_3, MSA, ammonia, amines or HOMs (R^2 for all <0.1). This is not to say that all of these molecules are not involved in the nucleation process, rather that elevations or reductions to their concentrations during nucleation periods do not have

https://doi.org/10.5194/acp-2020-84
Preprint. Discussion started: 4 March 2020
© Author(s) 2020. CC BY 4.0 License.

Atmospheric Chemistry and Physics Discussions

significant impact on NPF rates. In the example of alkylamines, their gas phase concentration may decrease due to clustering with elevated sulphuric acid (and therefore they will not be detectable as free amines), and losses due to enhanced photochemistry during the periods of highest NPF rate. Concentrations for these ions are shown in Figure S5. The strength of the relationship between sulphuric acid and nucleation rate has been quantitatively reproduced in chamber studies involving the H_2SO_4-H_2O-DMA, and H_2SO_4-H_2O-BioOxOrg system, accurately reproducing tropospheric observations of nucleation rates (Almeida et al., 2013; Riccobono et al., 2014). A comparison between our data and results from the CLOUD chamber is presented in Figure 5; included are the H_2SO_4-H_2O, H_2SO_4-NH_3-H_2O (Kirkby et al., 2011), H_2SO_4-H_2O-DMA (Almeida et al., 2013) and H_2SO_4-BioOxOrg-H_2O systems (Riccobono et al., 2014) – BioOxOrg refers to the oxidation products of pinanediol ($C_{10}H_{18}O_2$) and $OH^{\cdot}$. The relationship between sulphuric acid and nucleation rate is similar to the H_2SO_4-DMA-H_2SO_4 system, with extremely high nucleation rates compared to the other systems. The nucleation rate is also broadly similar also to the system involving BioOxOrg. No dissimilarity is seen between the data points corresponding to full or burst type nucleation, indicating similar mechanisms of formation, despite lower HOM concentrations on these days. No higher-order sulphuric acid clusters, sulphuric acid-base clusters, nor sulphuric acid-HOM clusters were visible in the mass spectral data, likely due to these being below the limit of detection of the instrument (Jokinen et al., 2012), so cluster identity cannot be directly identified. Sulfuric acid trimer stabilisation is dependent upon base abundance (Ortega et al 2012), and conversely, sensitivity of nitrate CI-APi-ToF to sulfuric acid-base clusters is reduced due to the high base content of such clusters (Jen et al., 2016).

To further explore the relationship between sulphuric acid clusters and the rate of nucleation, the sulphuric acid dimer:monomer ratio is plotted in Figure 6. Sulphuric acid dimer roughly represents the strength of sulphuric acid clustering in the nitrate CI-APi-ToF, as significant fragmentation of sulphuric acid-base clusters occurs upon charging, with evaporation of water and bases from the

https://doi.org/10.5194/acp-2020-84
Preprint. Discussion started: 4 March 2020
© Author(s) 2020. CC BY 4.0 License.

Atmospheric Chemistry and Physics Discussions

system (Ortega et al., 2012, 2014). Stronger bases result in more sulphuric acid dimer making it through the system, and thus this ratio is higher for systems involving bases that form stronger clusters with sulphuric acid. The dashed line represents the lower limit of sulphuric acid that would be seen due to ion induced clustering (IIC) in the nitrate chemical ionisation system (Zhao et al., 2010). The sulphuric acid dimer:monomer ratio seen in the CLOUD H_2SO_4-DMA-H_2O system is plotted, alongside our own data from Barcelona. The ratio from our own data is seen to be much lower than that for the system purely involving DMA as a ternary stabilising species. Similarly, this ratio is lower than for reports of H_2SO_4-DMA-H_2O nucleation in Shanghai (Yao et al., 2018), but is markedly similar to reports in central rural Germany (Kürten et al., 2016). Similar to central Germany, this ratio increases at lower sulphuric acid concentrations to a ratio more similar to the H_2SO_4-DMA-H_2O system. A possible explanation for this is that at higher sulphuric acid concentrations, the concentrations of stronger stabilising bases are insufficient to stabilise all present sulphuric acid, with the higher end of the sulphuric acid concentrations seen in this data roughly equivalent to 1 pptv sulphuric acid (3×10^7 cm^{-3} = 1.2 pptv sulphuric acid). We also cannot account for clustering due to naturally charged sulphuric acid in the atmosphere, but ion concentrations in urban environments tend to be small due to efficient sink processes (Hirsikko et al., 2011). Particle formation therefore plausibly operates by mechanisms similar to the H_2SO_4-DMA-H_2O and H_2SO_4-BioOxOrg-H_2O systems which may occur in parallel.

3.3 HOMs and Growth

Barcelona, as a densely populated urban agglomerate, is characterised by higher NO_x than the remote conditions under which HOMs have primarily been studied (Bianchi et al., 2016, 2017; Schobesberger et al., 2013; Yan et al., 2016). High insolation will also result in higher $HO_2^{\cdot}$, as well as higher $RO_2^{\cdot}$ and other radicals. NO_x, $HO_2^{\cdot}$ act as peroxy radical terminators, reducing the likelihood of autoxidation to produce high O:C molecules, and the likelihood of $RO_2^{\cdot}$-$RO_2^{\cdot}$ dimerization. The NO_x-$RO_2^{\cdot}$ reaction also produces HOMs with nitrate ester functionality (Brean et

https://doi.org/10.5194/acp-2020-84
Preprint. Discussion started: 4 March 2020
© Author(s) 2020. CC BY 4.0 License.

Atmospheric Chemistry and Physics Discussions

al., 2019; Garmash et al., 2019; Rissanen, 2018), which tend to have higher volatilities, and are less efficient at participating in early-stage NPF (Ehn et al., 2014; Lehtipalo et al., 2018), likely due to intramolecular H-bonding (Elm et al., 2017). This, combined with plentiful VOCs with carbon number <10 results in more volatile HOMs (see Figures S2 and S3) likely classed as LVOC or SVOC (Bianchi et al., 2019; Tröstl et al., 2016). HOMs of this volatility are mostly incapable of producing particles in the absence of sulphuric acid by ion-induced mechanisms observed in a chamber study and the remote environment (Kirkby et al., 2016; Rose et al., 2018). Peaks due to certain night-time HOMs are seen, largely C_{10} HOMs attributable to inland air masses (Querol et al., 2017). Many of these night-time C_{10} HOMs contain nitrogen functionalities, attributable to either oxidation by NO_3· radicals or NO_x chemistry and were not associated with night-time NPF. As shown in Figure 3, an elevated HOM concentration appears to be a necessary condition for particle growth past 10 nm during NPF events. These days are associated with elevated temperatures, solar radiation, higher ozone, and lower NO:NO_2 ratio. HIO_3 is also significantly higher on burst-event days, likely a function of air mass trajectory, as HIO_3 would not inhibit particle growth, condensational growth being a reversible, step-wise kinetic process. A recent study in a remote environment reports growth rates matching condensation rates without accounting for aqueous phase chemistry (Mohr et al., 2019). HOM yields are highly dependent upon temperature (Quéléver et al., 2019; Stolzenburg et al., 2018). Lower temperatures result in slower H-abstractions, which will result in the likelihood of an RO_2· to undergo a different reaction pathway, such as termination with HO_2· to increase (Praske et al., 2018). This is particularly important if there is a large energy barrier for the first or second H-abstraction taking place, as this will determine the number of hydrogen bond donating groups, and therefore whether the NO_3^- CI-APi-ToF is sensitive to a molecule or not. Figure 7(a) shows temperature plotted against the signal of HOMs. The precursors for these HOMs are presumed to be largely isoprene, alkylbenzenes and monoterpenes. The mean peak intensities assigned to alkylbenzene derived HOMs are approximately a factor of two higher than those assigned to isoprene and monoterpene oxidation across this entire campaign.

https://doi.org/10.5194/acp-2020-84
Preprint. Discussion started: 4 March 2020
© Author(s) 2020. CC BY 4.0 License.

Atmospheric Chemistry and Physics Discussions

337 In this data these VOCs are, with the exception of isoprene, not largely temperature dependent, with
338 many of these HOMs forming under negligible or zero insolation, and therefore very low $OH^{\cdot}$
339 concentrations. These nighttime HOMs will not be derived from the oxidation of aromatics,
340 however, as rates of oxidation of alkylbenzenes by O_3 and $NO_3^{\cdot}$ are negligible (Molteni et al, 2018).
341 These nighttime HOMs will therefore mostly be derived from biogenic emissions which undergo
342 more rapid nocturnal oxidation, and are likely transported inland by the land breeze during night
343 (Millán, 2014; Querol et al., 2017).
344
345 Operating under the assumption that C_5, C_7, and C_9 HOMs primarily arise from isoprene, toluene
346 and C_3-alkylbenzene oxidation respectively (Molteni et al., 2018; Wang et al., 2017), HOM signals
347 plotted against parent VOC concentration indicate their dependence upon that VOC. Here, a C_7
348 HOM is thought to follow the formula $C_7H_{8\text{-}12}O_{5\text{-}10}N_{0\text{-}2}$. This has been done in Figure 7(b). HOM
349 concentration is broadly dependent on VOC concentration. This is most significant for isoprene.
350 Fragmented monoterpene oxidation products will also contribute to the total number of C_9 HOMs,
351 and similarly, other VOCs can fragment upon oxidation. However, these results indicate that the
352 limiting factor in HOM production is temperature, and to a lesser degree VOC concentration.
353
354 Figure 8 shows three mass-defect plots for a non-event period, full-event period, and burst-event
355 period (event days are the same days as shown in Figure 1). Here, oxygenated volatile organic
356 compounds (OVOC) are defined as species visible in the nitrate CI-APi-ToF that do not classify as
357 HOM. Here, the detailed criteria provided by Bianchi et al. (2019) cannot be applied to define
358 HOM, as knowledge as to whether a molecule is a result of autoxidation requires sound knowledge
359 of the structure of the precursors present. The criteria of both containing 6 oxygen atoms and 5
360 carbon atoms or greater, and having an O:C ratio >0.6 is applied, as these molecules will all
361 plausibly fulfil the updated criteria of "HOM". The particular non-event day included in Figure 8
362 was characterised by lower solar radiation and temperatures than average, so lower signals for

https://doi.org/10.5194/acp-2020-84
Preprint. Discussion started: 4 March 2020
© Author(s) 2020. CC BY 4.0 License.

Atmospheric Chemistry and Physics Discussions

oxygenated species are seen due to weaker photochemistry (i.e., $OH^{\cdot}$ concentration), and slower autoxidation due to slower H-shift reactions (Frege et al., 2018; Quéléver et al., 2019; Stolzenburg et al., 2018). The full-event day sees enhancements to smaller OVOCs and HOMs compared to the non-event day, especially around 150-200 m/Q. Some of the largest peaks in the mass spectra correspond to formulae seen arising from the $OH^{\cdot}$ oxidation of alkylbenzenes (Molteni et al., 2018; Wang et al., 2017). Larger HOMs see a less significant enhancement to smaller alkylbenzene derived HOMs. Most significant is the presence of many larger, unidentified HOMs >500 m/Q. During full-event periods, these peaks are both more numerous, and larger. This area of the mass spectrum will compromise the largest HOMs, from oxidation of large VOCs or from the $RO_2^{\cdot}$ + $RO_2^{\cdot}$ dimerization reaction of two smaller $RO_2^{\cdot}$, these will likely have extremely low vapour pressures and be able to drive early stage particle growth (Mohr et al., 2019; Tröstl et al., 2016). The burst-event day has significantly lower concentrations of OVOCs and HOMs, and to a lesser degree, their nitrogen containing counterparts (N-OVOCs and N-HOMs), with significantly fewer compounds >500 m/Q. The most significant difference between the HOMs on both types of event days is the C_9 and C_{10} HOMs, consistent with lower concentrations of monoterpenes on burst-event days. The sulphur containing acids all have similar peak areas to the full-event day. These elevations to condensable HOMs on particle formation days with growth consistent with particle composition data as measured by ACSM, also showing a significant increase to organic mass concentration in the late evening (around when new particles reach sizes measurable by ACSM) and night on full-event days. This was not seen on days without nucleation, nor on days with nucleation but no growth (see Figure S4).

4. CONCLUSIONS

We show new particle formation rates in Barcelona are linearly dependent upon the sulphuric acid concentrations, and this mechanism plausibly proceeds by the formation of clusters involving sulphuric acid and highly oxygenated organic molecules, with likely involvement of bases. This

https://doi.org/10.5194/acp-2020-84
Preprint. Discussion started: 4 March 2020
© Author(s) 2020. CC BY 4.0 License.

Atmospheric Chemistry and Physics Discussions

multiplicity of mechanisms has been shown to occur in chamber studies but has not been observed in the real atmosphere previously. The rate of nucleation relative to sulphuric acid concentration is similar to observations of H_2SO_4-DMA-H_2O and H_2SO_4-BioOxOrg-H_2O nucleation. Nucleation rates seem independent of HOM concentrations, implying that these mechanisms may occur in competition with one another. The HOMs present in this study occur mostly from oxidation of alkylbenzenes and monoterpenes, with a strong dependence of their concentration on both temperature and VOC concentration. Concentrations of species associated with coastal and oceanic sources such as MSA and HIO_3 were low, even though NPF was consistently associated with southerly and south-westerly air masses, indicating that anthropogenic emissions of SO_2, (largely arising from shipping emissions in Barcelona) and aromatic organic compounds are more important precursors for compounds which intiate new particle formation and growth than oceanic emissions. High HOM signals are seen to be a necessary condition for new particle growth past 10 nm, and it is evident that HOM concentrations are dependent upon temperature and VOC precursor concentration. Specifically large HOMs of extremely low volatility >500 m/Q are absent in the mass spectra on these days without particle formation, as well as particle formation without growth.

These results are consistent with extensive chamber and flow tube studies on particle formation from sulphuric acid, amines and HOMs, and further, nucleation rates relative to sulphuric acid are similar to many tropospheric observations. Barcelona is representative of many Mediterranean urban environments, with moderate pollution, influence of shipping emissions, and high insolation, and thus the present study reveals the complexity of NPF mechanisms in these environments.

DATA AVAILABILITY

Data supporting this publication are openly available from the UBIRA eData repository at https://doi.org/10.25500/edata.bham.00000434

https://doi.org/10.5194/acp-2020-84
Preprint. Discussion started: 4 March 2020
© Author(s) 2020. CC BY 4.0 License.

Atmospheric Chemistry and Physics Discussions

AUTHOR CONTRIBUTIONS

RMH and XQ conceived the study, JB and DCSB carried out the APi-TOF and related measurements with assistance from AA and MCM. The VOC measurements were proposed by NM and collected by BT-R. JB wrote the first draft of the manuscript which was enhanced by contributions from the co-authors.

COMPETING INTERESTS

The authors have no conflict of interests.

ACKNOWLEDGEMENTS

Financial assistance from the Spanish Ministry of Science, Innovation and Universities and Competitiveness and FEDER funds under the project HOUSE (CGL2016-78594-R), and by the Generalitat de Catalunya (AGAUR 2017 SGR41) is gratefully acknowledged. MCM acknowledges the Ramón y Cajal Fellowship awarded by the Spanish Ministry. Financial support of the UK scientists by the Natural Environment Research Council through the National Centre for Atmospheric Science is also acknowledged (R8/H12/83/011).

https://doi.org/10.5194/acp-2020-84
Preprint. Discussion started: 4 March 2020
© Author(s) 2020. CC BY 4.0 License.

Atmospheric Chemistry and Physics Discussions

FIGURE LEGENDS:

Figure 1: Example SMPS contour plots of (a) non-event day, (b) full-event day and (c) burst-event day.

Figure 2: Box plots for days of non-event, full-event and burst-event, showing (a) condensation sink, (b) temperature, and (c) global radiation.

Figure 3: Box plots for days of non-event, full-event and burst-event, showing (a) sulphuric acid, (b) ammonia, C_2 and C_4 amines, as clustered with the nitrate dimer and trimer, and (c) summed HOM concentration from C_5+. Units for ammonia + amines are normalised counts, as no calibration was performed.

Figure 4: Formation rate (J_5) plotted against sulphuric acid monomer concentration, coloured by condensation sink. Circles represent burst-events, squares represent full events.

Figure 5: Formation rate ($J_{1.5}$) plotted against sulphuric acid monomer concentration for data collected from Barcelona. Tan circles represent burst-events, purple squares represent full events. as well as that for the H_2SO_4-H_2O (blue inverted triangles), H_2SO_4-NH_3-H_2O (yellow inverted triangles), H_2SO_4-DMA-H_2O (pink triangles), and H_2SO_4-BioOxOrg-H_2O (brown diamonds) systems from the CLOUD chamber (Almeida et al., 2013; Kirkby et al., 2011; Riccobono et al., 2014).

Figure 6: Sulphuric acid dimer concentration plotted against monomer concentration, showing burst-event periods (tan circles), full event periods (purple squares), non-event periods (green inverted triangles), and the ratio of sulphuric acid dimer:monomer in the CLOUD chamber for the H_2SO_4-H_2O-DMA system (pink triangles) (Almeida et al., 2013). Dashed line represents the lower limit of dimer concentration produced by ion induced clustering in the chemical ionization unit (Zhao et al., 2010).

Figure 7: Influencing factors on VOC concentration, showing (A) temperature plotted against $C_{5\text{-}10}$ HOM signal, coloured by global radiation, and (B) VOC concentration plotted against HOM signal. These are segregated by carbon number/VOC, i.e, C_7 HOMs plotted against toluene, under the assumption that toluene oxidation is the main producer of C_7 HOMs. Ellipses show 95% confidence on a multivariate t-distribution.

Figure 8: Mass defect plots for (a) non-event, (b) full-event, and (c) burst-event periods, data taken from 10:00 – 15:00 on the days 12/07/2018, 16/07/2018 and 15/07/2018 respectively. Size corresponds to mass spectral peak area. Ions are coloured according to identified chemical composition. *Blue* points correspond to HOMs containing all organic species with ≥5 carbon atoms and ≥6 oxygen atoms, and an O:C ratio of >0.6. *Purple* points correspond to the same but for species containing 1-2 nitrogen atoms. Species not meeting this HOM criterea were classed generally as OVOCs which are coloured *brown*, with the nitrogen containing OVOCs coloured *orange*. Sulphur acids (*red*) include ions HSO_4^-, $CH_3SO_3^-$ and SO_5^-, as well as the sulphuric acid dimer. Iodine acids (*green*) contains both IO_3^- and I^- (the latter presumably deprotonated hydrogen iodide). Unidentified points are left uncoloured.

https://doi.org/10.5194/acp-2020-84
Preprint. Discussion started: 4 March 2020
© Author(s) 2020. CC BY 4.0 License.

Atmospheric Chemistry and Physics Discussions

REFERENCES

Ábalos, M., Bayona, J. M. and Ventura, F.: Development of a solid-phase microextraction GC-NPD procedure for the determination of free volatile amines in wastewater and sewage-polluted waters, Anal. Chem., 71(16), 3531–3537, doi:10.1021/ac990197h, 1999.

Agudelo-Castañeda, D. M., Teixeira, E. C., Braga, M., Rolim, S. B. A., Silva, L. F. O., Beddows, D. C. S., Harrison, R. M. and Querol, X.: Cluster analysis of urban ultrafine particles size distributions, Atmos. Pollut. Res., 10(1), 45–52, doi:10.1016/j.apr.2018.06.006, 2019.

Almeida, J., Schobesberger, S., Kürten, A., Ortega, I. K., Kupiainen-Määttä, O., Praplan, A. P., Adamov, A., Amorim, A., Bianchi, F., Breitenlechner, M., David, A., Dommen, J., Donahue, N. M., Downard, A., Dunne, E., Duplissy, J., Ehrhart, S., Flagan, R. C., Franchin, A., Guida, R., Hakala, J., Hansel, A., Heinritzi, M., Henschel, H., Jokinen, T., Junninen, H., Kajos, M., Kangasluoma, J., Keskinen, H., Kupc, A., Kurtén, T., Kvashin, A. N., Laaksonen, A., Lehtipalo, K., Leiminger, M., Leppä, J., Loukonen, V., Makhmutov, V., Mathot, S., McGrath, M. J., Nieminen, T., Olenius, T., Onnela, A., Petäjä, T., Riccobono, F., Riipinen, I., Rissanen, M., Rondo, L., Ruuskanen, T., Santos, F. D., Sarnela, N., Schallhart, S., Schnitzhofer, R., Seinfeld, J. H., Simon, M., Sipilä, M., Stozhkov, Y., Stratmann, F., Tomé, A., Tröstl, J., Tsagkogeorgas, G., Vaattovaara, P., Viisanen, Y., Virtanen, A., Vrtala, A., Wagner, P. E., Weingartner, E., Wex, H., Williamson, C., Wimmer, D., Ye, P., Yli-Juuti, T., Carslaw, K. S., Kulmala, M., Curtius, J., Baltensperger, U., Worsnop, D. R., Vehkamäki, H. and Kirkby, J.: Molecular understanding of sulphuric acid-amine particle nucleation in the atmosphere, Nature, 502(7471), 359–363, doi:10.1038/nature12663, 2013.

Bianchi, F., Tröstl, J., Junninen, H., Frege, C., Henne, S., Hoyle, C. R., Molteni, U., Herrmann, E., Bukowiecki, N., Chen, X., Duplissy, J., Gysel, M., Hutterli, M., Kangasluoma, J., Kontkanen, J., Manninen, H. E., Münch, S., Peräkylä, O., Petäjä, T., Rondo, L., Williamson, C., Weingartner, E., Worsnop, D. R., Kulmala, M., Dommen, J. and Baltensperger, U.: New particle formation in the free troposphere : A question of chemistry and timing, Science (80-.)., 5456(May), 1–11, 2016.

Bianchi, F., Garmash, O., He, X., Yan, C., Iyer, S., Rosendahl, I., Xu, Z., Rissanen, M. P., Riva, M., Taipale, R., Sarnela, N., Petäjä, T., Worsnop, D. R., Kulmala, M., Ehn, M. and Junninen, H.: The role of highly oxygenated molecules (HOMs) in determining the composition of ambient ions in the boreal forest, Atmos. Chem. Phys., 17(22), 13819–13831, doi:10.5194/acp-17-13819-2017, 2017.

Bianchi, F., Kurtén, T., Riva, M., Mohr, C., Rissanen, M. P., Roldin, P., Berndt, T., Crounse, J. D., Wennberg, P. O., Mentel, T. F., Wildt, J., Junninen, H., Jokinen, T., Kulmala, M., Worsnop, D. R., Thornton, J. A., Donahue, N., Kjaergaard, H. G. and Ehn, M.: Highly Oxygenated Organic Molecules (HOM) from Gas-Phase Autoxidation Involving Peroxy Radicals: A Key Contributor to Atmospheric Aerosol, Chem. Rev., 2019.

Bousiotis, D., Dall'osto, M., Beddows, D. C. S., Pope, F. D. and Harrison, R. M.: Analysis of new particle formation (NPF) events at nearby rural, urban background and urban roadside sites, Atmos. Chem. Phys, 19, 5679–5694, doi:10.5194/acp-19-5679-2019, 2019.

Brean, J., Harrison, R. M., Shi, Z., Beddows, D. C. S., W Joe, A. F. and Nicholas Hewitt, C.: Observations of highly oxidised molecules and particle nucleation in the atmosphere of Beijing, Atmos. Chem. Phys. Discuss., (March), 1–35, doi:10.5194/acp-2019-156, 2019.

Brines, M., Dall'Osto, M., Beddows, D. C. S., Harrison, R. M., and Querol, X.: Simplifying aerosol size distributions modes simultaneously detected at four monitoring sites during SAPUSS, Atmos. Chem. Phys., 14, 2973–2986, https://doi.org/10.5194/acp-14-2973-2014, 2014.

https://doi.org/10.5194/acp-2020-84
Preprint. Discussion started: 4 March 2020
© Author(s) 2020. CC BY 4.0 License.

Brines, M., Dall'Osto, M., Beddows, D. C. S., Harrison, R. M., Gómez-Moreno, F., Núñez, L., Artíñano, B., Costabile, F., Gobbi, G. P., Salimi, F., Morawska, L., Sioutas, C., and Querol, X.: Traffic and nucleation events as main sources of ultrafine particles in high-insolation developed world cities, Atmos. Chem. Phys., 15, 5929–5945, https://doi.org/10.5194/acp-15-5929-2015, 2015.

Cadle, S. H. and Mulawa, P. A.: Low-molecular-weight aliphatic amines in exhaust from catalyst-equipped cars, Environ. Sci. Technol., 14(6), 718–723, doi:10.1021/es60166a011, 1980.

Carnerero, C., Pérez, N., Petäjä, T., Laurila, T. M., Ahonen, L. R., Kontkanen, J., Ahn, K. H., Alastuey, A. and Querol, X.: Relating high ozone, ultrafine particles, and new particle formation episodes using cluster analysis, Atmos. Environ. X, 4(May), 1–20, doi:10.1016/j.aeaoa.2019.100051, 2019.

Cohen, A. J., Brauer, M., Burnett, R., Anderson, H. R., Frostad, J., Estep, K., Balakrishnan, K., Brunekreef, B., Dandona, L., Dandona, R., Feigin, V., Freedman, G., Hubbell, B., Jobling, A., Kan, H., Knibbs, L., Liu, Y., Martin, R., Morawska, L., Pope, C. A., Shin, H., Straif, K., Shaddick, G., Thomas, M., van Dingenen, R., van Donkelaar, A., Vos, T., Murray, C. J. L. and Forouzanfar, M. H.: Estimates and 25-year trends of the global burden of disease attributable to ambient air pollution: an analysis of data from the Global Burden of Diseases Study 2015, Lancet, 389(10082), 1907–1918, doi:10.1016/S0140-6736(17)30505-6, 2017.

Cubison, M. J. and Jimenez, J. L.: Statistical precision of the intensities retrieved from constrained fitting of overlapping peaks in high-resolution mass spectra, Atmos. Meas. Tech., 8(6), 2333–2345, doi:10.5194/amt-8-2333-2015, 2015.

Dal Maso, M., Kulmala, M., Riipinen, I., Wagner, R., Hussein, T., Aalto, P. P. and Lehtinen, K. E. J.: Formation and growth of fresh atmospheric aerosols: Eight years of aerosol size distribution data from SMEAR II, Hyytiälä, Finland, Boreal Environ. Res., 10(5), 323–336, 2005.

Dall'Osto, M., Querol, X., Alastuey, A., O'Dowd, C., Harrison, R. M., Wenger, J. and Gómez-Moreno, F. J.: On the spatial distribution and evolution of ultrafine particles in Barcelona, Atmos. Chem. Phys., 13(2), 741–759, doi:10.5194/acp-13-741-2013, 2013.

Ehn, M., Thornton, J. A., Kleist, E., Sipilä, M., Junninen, H., Pullinen, I., Springer, M., Rubach, F., Tillmann, R., Lee, B., Lopez-Hilfiker, F., Andres, S., Acir, I.-H., Rissanen, M., Jokinen, T., Schobesberger, S., Kangasluoma, J., Kontkanen, J., Nieminen, T., Kurtén, T., Nielsen, L. B., Jørgensen, S., Kjaergaard, H. G., Canagaratna, M., Maso, M. D., Berndt, T., Petäjä, T., Wahner, A., Kerminen, V.-M., Kulmala, M., Worsnop, D. R., Wildt, J. and Mentel, T. F.: A large source of low-volatility secondary organic aerosol, Nature, 506(7489), 476–479, doi:10.1038/nature13032, 2014.

Elm, J., Myllys, N. and Kurtén, T.: What is Required for Highly Oxidized Molecules to Form Clusters with Sulphuric Acid?, J. Phys. Chem. A, 121(23), 4578–4587, doi:10.1021/acs.jpca.7b03759, 2017.

Frege, C., Ortega, I. K., Rissanen, M. P., Praplan, A. P., Steiner, G., Heinritzi, M., Ahonen, L., Amorim, A., Bernhammer, A. K., Bianchi, F., Brilke, S., Breitenlechner, M., Dada, L., Dias, A., Duplissy, J., Ehrhart, S., El-Haddad, I., Fischer, L., Fuchs, C., Garmash, O., Gonin, M., Hansel, A., Hoyle, C. R., Jokinen, T., Junninen, H., Kirkby, J., Kürten, A., Lehtipalo, K., Leiminger, M., Lee Mauldin, R., Molteni, U., Nichman, L., Petäjä, T., Sarnela, N., Schobesberger, S., Simon, M., Sipilä, M., Stolzenburg, D., Tomé, A., Vogel, A. L., Wagner, A. C., Wagner, R., Xiao, M., Yan, C., Ye, P., Curtius, J., Donahue, N. M., Flagan, R. C., Kulmala, M., Worsnop, D. R., Winkler, P., Dommen, J.

https://doi.org/10.5194/acp-2020-84
Preprint. Discussion started: 4 March 2020
© Author(s) 2020. CC BY 4.0 License.

Atmospheric Chemistry and Physics Discussions

585 and Baltensperger, U.: Influence of temperature on the molecular composition of ions and charged
586 clusters during pure biogenic nucleation, Atmos. Chem. Phys., 18(1), 65–79, doi:10.5194/acp-18-65-
587 2018, 2018.
588
589 Garmash, O., Rissanen, M. P., Pullinen, I., Schmitt, S., Kausiala, O., Tillmann, R., Percival, C.,
590 Bannan, T. J., Priestley, M., Hallquist, A. M., Kleist, E., Kiendler-scharr, A., Hallquist, M., Berndt,
591 T., Mcfiggans, G., Wildt, J., Mentel, T. and Ehn, M.: Multi-generation OH oxidation as a source for
592 highly oxygenated organic molecules from aromatics, Atmos. Chem. Phys. Discuss., (June), 1–33,
593 2019.
594 Ge, X., Wexler, A. S. and Clegg, S. L.: Atmospheric amines - Part I. A review, Atmos. Environ.,
595 45(3), 524–546, doi:10.1016/j.atmosenv.2010.10.012, 2011.
596
597 Glasoe, W. A., Volz, K., Panta, B., Freshour, N., Bachman, R., Hanson, D. R., Mcmurry, P. H. and
598 Jen, C.: Sulphuric acid nucleation: An experimental study of the effect of seven bases, J. Geophys.
599 Res. Atmos., 175(120), 1933–1950, doi:10.1038/175238c0, 2015.
600
601 Graus, M., Müller, M. and Hansel, A.: High resolution PTR-TOF: Quantification and Formula
602 Confirmation of VOC in Real Time, J. Am. Soc. Mass Spectrom., 21(6), 1037–1044,
603 doi:10.1016/j.jasms.2010.02.006, 2010.
604
605 Guo, S., Hu, M., Zamora, M. L., Peng, J., Shang, D., Zheng, J., Du, Z., Wu, Z., Shao, M., Zeng, L.,
606 Molina, M. J. and Zhang, R.: Elucidating severe urban haze formation in China., Proc. Natl. Acad.
607 Sci. U. S. A., 111(49), 17373–8, doi:10.1073/pnas.1419604111, 2014.
608
609 Harrison, R. M., Rob Mackenzie, A., Xu, H., Alam, M. S., Nikolova, I., Zhong, J., Singh, A., Zeraati-
610 Rezaei, S., Stark, C., Beddows, D. C. S., Liang, Z., Xu, R. and Cai, X.: Diesel exhaust nanoparticles
611 and their behaviour in the atmosphere, Proc. R. Soc. A Math. Phys. Eng. Sci., 474(2220),
612 doi:10.1098/rspa.2018.0492, 2018.
613
614 Henschel, S., Querol, X., Atkinson, R., Pandolfi, M., Zeka, A., Tertre, A. L., Analistis, A.,
615 Katsouyanni, K., Chanel, O., Pascal, M., Bouland, C., Haluza, D., Medina, S., and Goodman, P. G.:
616 Ambient air SO2 patterns in 6 European cities, Atmos. Environ., 79, 236–247,
617 https://doi.org/10.1016/j.atmosenv.2013.06.008, 2013.
618
619 Hirsikko, A., Nieminen, T., Gagné, S., Lehtipalo, K., Manninen, H. E., Ehn, M., Hõrrak, U.,
620 Kerminen, V.-M., Laakso, L., Mcmurry, P. H., Mirme, A., Mirme, S., Petäjä, T., Tammet, H.,
621 Vakkari, V., Vana, M. and Kulmala, M.: Atmospheric ions and nucleation: a review of observations,
622 Atmos. Chem. Phys, 11, 767–798, doi:10.5194/acp-11-767-2011, 2011.
623
624 Hutchinson, G. L., Mosier, A. R. and Andre, C. E.: Ammonia and Amine Emissions from a Large
625 Cattle Feedlot, J. Environ. Qual., 11(2), 288–293, 1982.
626
627 Hyttinen, N., Kupiainen-Määtta, O., Rissanen, M. P., Muuronen, M., Ehn, M. and Kurtén, T.:
628 Modeling the Charging of Highly Oxidized Cyclohexene Ozonolysis Products Using Nitrate-Based
629 Chemical Ionization, J. Phys. Chem. A, 119(24), 6339–6345, doi:10.1021/acs.jpca.5b01818, 2015.
630
631 IPCC, 2013: Climate Change 2013: The Physical Science Basis. Contribution of Working Group I to
632 the Fifth Assessment Report of the Intergovernmental Panel on Climate Change, edited by V. B. and
633 P. M. M. Stocker, T.F., D. Qin, G.-K. Plattner, M. Tignor, S.K. Allen, J. Boschung, A. Nauels, Y.
634 Xia, Cambridge University Press, Cambridge., 2014.
635
636 Jen, C. N., Zhao, J., McMurry, P. H., and Hanson, D. R.: Chemical ionization of clusters formed from

https://doi.org/10.5194/acp-2020-84
Preprint. Discussion started: 4 March 2020
© Author(s) 2020. CC BY 4.0 License.

Atmospheric Chemistry and Physics Discussions

637 sulfuric acid and dimethylamine or diamines, Atmos. Chem. Phys., 16, 12513–12529,
638 https://doi.org/10.5194/acp-16-12513-2016, 2016.
639
640 Jokinen, T., Sipilä, M., Junninen, H., Ehn, M., Lönn, G., Hakala, J., Petäjä, T., Mauldin, R. L.,
641 Kulmala, M. and Worsnop, D. R.: Atmospheric sulphuric acid and neutral cluster measurements using
642 CI-APi-TOF, Atmos. Chem. Phys., 12(9), 4117–4125, doi:10.5194/acp-12-4117-2012, 2012.
643
644 Jokinen, T., Sipilä, M., Kontkanen, J., Vakkari, V., Tisler, P., Duplissy, E.-M., Junninen, H.,
645 Kangasluoma, J., Manninen, H. E., Petäjä, T., Kulmala, M., Worsnop, D. R., Kirkby, J., Virkkula, A.
646 and Kerminen, V.-M.: Ion-induced sulphuric acid–ammonia nucleation drives particle formation in
647 coastal Antarctica, Sci. Adv., 4(11), eaat9744, doi:10.1126/sciadv.aat9744, 2018.
648
649 Junninen, H., Ehn, M., Petäjä, Luosujärvi, L., Kotiaho, T., Kostiainen, R., Rohner, U., Gonin, M.,
650 Fuhrer, K., Kulmala, M. and Worsnop, D. R.: A high-resolution mass spectrometer to measure
651 atmospheric ion composition, Atmos. Meas. Tech., 3(4), 1039–1053, doi:10.5194/amt-3-1039-2010,
652 2010.
653
654 Kerminen, V. M., Chen, X., Vakkari, V., Petäjä, T., Kulmala, M. and Bianchi, F.: Atmospheric new
655 particle formation and growth: Review of field observations, Environ. Res. Lett., 13(10),
656 doi:10.1088/1748-9326/aadf3c, 2018.
657
658 Kirkby, J., Curtius, J., Almeida, J., Dunne, E., Duplissy, J., Ehrhart, S., Franchin, A., Gagné, S., Ickes,
659 L., Kürten, A., Kupc, A., Metzger, A., Riccobono, F., Rondo, L., Schobesberger, S., Tsagkogeorgas,
660 G., Wimmer, D., Amorim, A., Bianchi, F., Breitenlechner, M., David, A., Dommen, J., Downard, A.,
661 Ehn, M., Flagan, R. C., Haider, S., Hansel, A., Hauser, D., Jud, W., Junninen, H., Kreissl, F., Kvashin,
662 A., Laaksonen, A., Lehtipalo, K., Lima, J., Lovejoy, E. R., Makhmutov, V., Mathot, S., Mikkilä, J.,
663 Minginette, P., Mogo, S., Nieminen, T., Onnela, A., Pereira, P., Petäjä, T., Schnitzhofer, R., Seinfeld,
664 J. H., Sipilä, M., Stozhkov, Y., Stratmann, F., Tomé, A., Vanhanen, J., Viisanen, Y., Vrtala, A.,
665 Wagner, P. E., Walther, H., Weingartner, E., Wex, H., Winkler, P. M., Carslaw, K. S., Worsnop, D.
666 R., Baltensperger, U. and Kulmala, M.: Role of sulphuric acid, ammonia and galactic cosmic rays in
667 atmospheric aerosol nucleation, Nature, 476(7361), 429–435, doi:10.1038/nature10343, 2011.
668
669 Kirkby, J., Duplissy, J., Sengupta, K., Frege, C., Gordon, H., Williamson, C., Heinritzi, M., Simon,
670 M., Yan, C., Almeida, J., Trostl, J., Nieminen, T., Ortega, I. K., Wagner, R., Adamov, A., Amorim,
671 A., Bernhammer, A. K., Bianchi, F., Breitenlechner, M., Brilke, S., Chen, X., Craven, J., Dias, A.,
672 Ehrhart, S., Flagan, R. C., Franchin, A., Fuchs, C., Guida, R., Hakala, J., Hoyle, C. R., Jokinen, T.,
673 Junninen, H., Kangasluoma, J., Kim, J., Krapf, M., Kurten, A., Laaksonen, A., Lehtipalo, K.,
674 Makhmutov, V., Mathot, S., Molteni, U., Onnela, A., Perakyla, O., Piel, F., Petaja, T., Praplan, A. P.,
675 Pringle, K., Rap, A., Richards, N. A. D., Riipinen, I., Rissanen, M. P., Rondo, L., Sarnela, N.,
676 Schobesberger, S., Scott, C. E., Seinfeld, J. H., Sipila, M., Steiner, G., Stozhkov, Y., Stratmann, F.,
677 Tomé, A., Virtanen, A., Vogel, A. L., Wagner, A. C., Wagner, P. E., Weingartner, E., Wimmer, D.,
678 Winkler, P. M., Ye, P., Zhang, X., Hansel, A., Dommen, J., Donahue, N. M., Worsnop, D. R.,
679 Baltensperger, U., Kulmala, M., Carslaw, K. S. and Curtius, J.: Ion-induced nucleation of pure
680 biogenic particles, Nature, 533(7604), 521–526, doi:10.1038/nature17953, 2016.
681
682 Kulmala, M., Dal Maso, M., Mäkelä, J. M., Pirjola, L., Väkevä, M., Aalto, P., Miikkulainen, P.,
683 Hämeri, K. and O'Dowd, C. D.: On the formation, growth and composition of nucleation mode
684 particles, Tellus, Ser. B Chem. Phys. Meteorol., 53(4), 479–490, doi:10.1034/j.1600-0889.2001.d01-
685 33.x, 2001.
686
687 Kulmala, M., Petäjä, T., Nieminen, T., Sipilä, M., Manninen, H. E., Lehtipalo, K., Dal Maso, M.,
688 Aalto, P. P., Junninen, H., Paasonen, P., Riipinen, I., Lehtinen, K. E. J., Laaksonen, A. and Kerminen,

https://doi.org/10.5194/acp-2020-84
Preprint. Discussion started: 4 March 2020
© Author(s) 2020. CC BY 4.0 License.

Atmospheric Chemistry and Physics Discussions

V.-M.: Measurement of the nucleation of atmospheric aerosol particles, Nat. Protoc., 7(9), 1651–1667, doi:10.1038/nprot.2012.091, 2012.

Kürten, A., Bergen, A., Heinritzi, M., Leiminger, M., Lorenz, V., Piel, F., Simon, M., Sitals, R., Wagner, A. C. and Curtius, J.: Observation of new particle formation and measurement of sulphuric acid, ammonia, amines and highly oxidized organic molecules at a rural site in central Germany, Atmos. Chem. Phys., 16(19), 12793–12813, doi:10.5194/acp-16-12793-2016, 2016.

Kurtén, T., Loukonen, V., Vehkaméki, H. and Kulmala, M.: Amines are likely to enhance neutral and ion-induced sulphuric acid-water nucleation in the atmosphere more effectively than ammonia, Atmos. Chem. Phys., 8(14), 4095–4103, doi:10.5194/acp-8-4095-2008, 2008.

Lee, S. H., Gordon, H., Yu, H., Lehtipalo, K., Haley, R., Li, Y. and Zhang, R.: New Particle Formation in the Atmosphere: From Molecular Clusters to Global Climate, J. Geophys. Res. Atmos., doi:10.1029/2018JD029356, 2019.

Lehtipalo, K., Yan, C., Dada, L., Bianchi, F., Xiao, M., Wagner, R., Stolzenburg, D., Ahonen, L. R., Amorim, A., Baccarini, A., Bauer, P. S., Baumgartner, B., Bergen, A., Bernhammer, A.-K., Breitenlechner, M., Brilke, S., Buchholz, A., Mazon, S. B., Chen, D., Chen, X., Dias, A., Dommen, J., Draper, D. C., Duplissy, J., Ehn, M., Finkenzeller, H., Fischer, L., Frege, C., Fuchs, C., Garmash, O., Gordon, H., Hakala, J., He, X., Heikkinen, L., Heinritzi, M., Helm, J. C., Hofbauer, V., Hoyle, C. R., Jokinen, T., Kangasluoma, J., Kerminen, V.-M., Kim, C., Kirkby, J., Kontkanen, J., Kürten, A., Lawler, M. J., Mai, H., Mathot, S., Mauldin, R. L., Molteni, U., Nichman, L., Nie, W., Nieminen, T., Ojdanic, A., Onnela, A., Passananti, M., Petäjä, T., Piel, F., Pospisilova, V., Quéléver, L. L. J., Rissanen, M. P., Rose, C., Sarnela, N., Schallhart, S., Schuchmann, S., Sengupta, K., Simon, M., Sipilä, M., Tauber, C., Tomé, A., Tröstl, J., Väisänen, O., Vogel, A. L., Volkamer, R., Wagner, A. C., Wang, M., Weitz, L., Wimmer, D., Ye, P., Ylisirniö, A., Zha, Q., Carslaw, K. S., Curtius, J., Donahue, N. M., Flagan, R. C., Hansel, A., Riipinen, I., Virtanen, A., Winkler, P. M., Baltensperger, U., Kulmala, M. and Worsnop, D. R.: Multicomponent new particle formation from sulphuric acid, ammonia, and biogenic vapors, Sci. Adv., 4(12), eaau5363, doi:10.1126/sciadv.aau5363, 2018.

Mikkonen, S., Romakkaniemi, S., Smith, J. N., Korhonen, H., Petäjä, T., Plass-Duelmer, C., Boy, M., McMurry, P. H., Lehtinen, K. E. J., Joutsensaari, J., Hamed, A., Mauldin, R. L., Birmili, W., Spindler, G., Arnold, F., Kulmala, M. and Laaksonen, A.: A statistical proxy for sulphuric acid concentration, Atmos. Chem. Phys., 11(21), 11319–11334, doi:10.5194/acp-11-11319-2011, 2011.

Millán, M.: Extreme hydrometeorological events and climate change predictions in Europe, J. Hydrol., 518(PB), 206–224, doi:10.1016/j.jhydrol.2013.12.041, 2014.

Miller, M. R., Raftis, J. B., Langrish, J. P., McLean, S. G., Samutrtai, P., Connell, S. P., Wilson, S., Vesey, A. T., Fokkens, P. H. B., Boere, A. J. F., Krystek, P., Campbell, C. J., Hadoke, P. W. F., Donaldson, K., Cassee, F. R., Newby, D. E., Duffin, R. and Mills, N. L.: Inhaled Nanoparticles Accumulate at Sites of Vascular Disease, ACS Nano, 11(5), 4542–4552, doi:10.1021/acsnano.6b08551, 2017.

Minguillón, M. C., Brines, M., Pérez, N., Reche, C., Pandol, M., Fonseca, A. S., Amato, F., Alastuey, A., Lyasota, A., Codina, B., Lee, H., Eun, H., Ahn, K. and Querol, X.: New particle formation at ground level and in the vertical column over the Barcelona area, , 165, 118–130, doi:10.1016/j.atmosres.2015.05.003, 2015.

Minguillón, M.C., Pérez, N., Marchand, N., Bertrand, A., Temime-Roussel, B., Agrios, K., Szidat,

https://doi.org/10.5194/acp-2020-84
Preprint. Discussion started: 4 March 2020
© Author(s) 2020. CC BY 4.0 License.

741 S., van Drooge, B.L., Sylvestre, A., Alastuey, A., Reche, C., Ripoll, A., Marco, E., Grimalt, J.O.,
742 Querol, X.: Secondary organic aerosol origin in an urban environment. Influence of biogenic and fuel
743 combustion precursors. Faraday Discuss., 189, 337-359, 2016.
744
745 Mohr, C., Thornton, J. A., Heitto, A., Lopez-Hilfiker, F. D., Lutz, A., Riipinen, I., Hong, J., Donahue,
746 N. M., Hallquist, M., Petäjä, T., Kulmala, M. and Yli-Juuti, T.: Molecular identification of organic
747 vapors driving atmospheric nanoparticle growth, Nat. Commun., 10(1), 1–7, doi:10.1038/s41467-
748 019-12473-2, 2019.
749
750 Møller, K. H., Tram, C. M. and Kjaergaard, H. G.: Side-by-Side Comparison of Hydroperoxide and
751 Corresponding Alcohol as Hydrogen-Bond Donors, J. Phys. Chem. A, 121(15), 2951–2959,
752 doi:10.1021/acs.jpca.7b01323, 2017.
753
754 Molteni, U., Bianchi, F., Klein, F., El Haddad, I., Frege, C., Rossi, M. J., Dommen, J. and
755 Baltensperger, U.: Formation of highly oxygenated organic molecules from aromatic compounds,
756 Atmos. Chem. Phys., 18(3), 1909–1921, doi:10.5194/acp-18-1909-2018, 2018.
757
758 Ng, N. L., Herndon, S. C., Trimborn, A., Canagaratna, M. R., Croteau, P. L., Onasch, T. B., Sueper,
759 D., Worsnop, D. R., Zhang, Q., Sun, Y. L. and Jayne, J. T.: An Aerosol Chemical Speciation Monitor
760 (ACSM) for routine monitoring of the composition and mass concentrations of ambient aerosol,
761 Aerosol Sci. Technol., 45(7), 770–784, doi:10.1080/02786826.2011.560211, 2011.
762
763 Olin, M., Kuuluvainen, H., Aurela, M., Kalliokoski, J., Kuittinen, N., Isotalo, M., Timonen, H. J.,
764 Niemi, J. V., Rönkkö, T., and Dal Maso, M.: Traffic-originated nanocluster emission exceeds
765 H2SO4-driven photochemical new particle formation in an urban area, Atmos. Chem. Phys., 20, 1–
766 13, https://doi.org/10.5194/acp-20-1-2020, 2020.
767
768 Ortega, I. K., Olenius, T., Kupiainen-Määttä, O., Loukonen, V., Kurtén, T., and Vehkamäki, H.:
769 Electrical charging changes the composition of sulfuric acid–ammonia/dimethylamine clusters,
770 Atmos. Chem. Phys., 14, 7995–8007, https://doi.org/10.5194/acp-14-7995-2014, 2014.
771
772 Pandolfi, M., Amato, F., Reche, C., Alastuey, A., Otjes, R. P., Blom, M. J. and Querol, X.: Summer
773 ammonia measurements in a densely populated Mediterranean city, Atmos. Chem. Phys., 12(16),
774 7557–7575, doi:10.5194/acp-12-7557-2012, 2012.
775
776 Penner, J. E., Xu, L. and Wang, M.: Satellite methods underestimate indirect climate forcing by
777 aerosols., Proc. Natl. Acad. Sci. U. S. A., 108(33), 13404–13408, doi:10.1073/pnas.1018526108,
778 2011.
779 Praske, E., Otkjær, R. V., Crounse, J. D., Hethcox, J. C., Stoltz, B. M., Kjaergaard, H. G. and
780 Wennberg, P. O.: Atmospheric autoxidation is increasingly important in urban and suburban North
781 America, Proc. Natl. Acad. Sci., 115(1), 64–69, doi:10.1073/pnas.1715540115, 2018.
782
783 Quéléver, L. L. J., Kristensen, K., Normann Jensen, L., Rosati, B., Teiwes, R., Daellenbach, K. R.,
784 Peräkylä, O., Roldin, P., Bossi, R., Pedersen, H. B., Glasius, M., Bilde, M. and Ehn, M.: Effect of
785 temperature on the formation of highly oxygenated organic molecules (HOMs) from alpha-pinene
786 ozonolysis, Atmos. Chem. Phys, 19, 7609–7625, doi:10.5194/acp-19-7609-2019, 2019.
787 Querol, X., Gangoiti, G., Mantilla, E., Alastuey, A., Minguillón, M. C., Amato, F., Reche, C., Viana,
788 M., Moreno, T., Karanasiou, A., Rivas, I., Pérez, N., Ripoll, A., Brines, M., Ealo, M., Pandolfi, M.,
789 Lee, H. K., Eun, H. R., Park, Y. H., Escudero, M., Beddows, D., Harrison, R. M., Bertrand, A.,
790 Marchand, N., Lyasota, A., Codina, B., Olid, M., Udina, M., Jiménez-Esteve, B., Jiménez-Esteve, B.
791 B., Alonso, L., Millán, M. and Ahn, K. H.: Phenomenology of high-ozone episodes in NE Spain,
792 Atmos. Chem. Phys., 17(4), 2817–2838, doi:10.5194/acp-17-2817-2017, 2017.

https://doi.org/10.5194/acp-2020-84
Preprint. Discussion started: 4 March 2020
© Author(s) 2020. CC BY 4.0 License.

Reche, C., Viana, M., Karanasiou, A., Cusack, M., Alastuey, A., Artiñano, B., Revuelta, M. A., López-Mahía, P., Blanco-Heras, G., Rodríguez, S., Sánchez de la Campa, A. M., Fernández-Camacho, R., González-Castanedo, Y., Mantilla, E., Tang, Y. S. and Querol, X.: Urban NH3 levels and sources in six major Spanish cities, Chemosphere, 119, 769–777, doi:10.1016/j.chemosphere.2014.07.097, 2015.

Riccobono, F., Schobesberger, S., Scott, C., Dommen, J., Ortega, I., Rondo, L., Almeida, J., Amorim, A., Bianchi, F., Breitenlechner, M., David, A., Downard, A., Dunne, E., Duplissy, J., Ehrhart, S., Flagan, R., Franchin, A., Hansel, A., Junninen, H., Kajos, M., Keskinen, H., Kupc, A., Kürten, A., Kvashin, A., Laaksonen, A., Lehtipalo, K., Makhmutov, V., Mathot, S., Nieminen, T., Onnela, A., Petäjä, T., Praplan, A., Santos, F., Schallhart, S., Seinfeld, J., Sipilä, M., Van Spracklen, D., Stozhkov, Y., Stratmann, F., Tomé, A., Tsagkogeorgas, G., Vaattovaara, P., Viisanen, Y., Vrtala, A., Wagner, P., Weingartner, E., Wex, H., Wimmer, D., Carslaw, K., Curtius, J., Donahue, N., Kirkby, J., Kulmala, M., Worsnop, D. and Baltensperger, U.: Oxidation products of biogenic emissions contribute to nucleation of atmospheric particles., Science (80-.)., 344(6185), 717–721, doi:10.1126/science.1243527, 2014.

Rissanen, M. P.: NO2 Suppression of Autoxidation-Inhibition of Gas-Phase Highly Oxidized Dimer Product Formation, ACS Earth Sp. Chem., 2(11), 1211–1219, doi:10.1021/acsearthspacechem.8b00123, 2018.

Rose, C., Zha, Q., Dada, L., Yan, C., Lehtipalo, K., Junninen, H., Mazon, S. B., Jokinen, T., Sarnela, N., Sipilä, M., Petäjä, T., Kerminen, V.-M., Bianchi, F. and Kulmala, M.: Observations of biogenic ion-induced cluster formation in the atmosphere, Sci. Adv., 4(4), 5218, doi:10.1126/sciadv.aar5218, 2018.

Schobesberger, S., Junninen, H., Bianchi, F., Lönn, G., Ehn, M., Lehtipalo, K., Dommen, J., Ehrhart, S., Ortega, I. K., Franchin, A., Nieminen, T., Riccobono, F., Hutterli, M., Duplissy, J., Almeida, J., Amorim, A., Breitenlechner, M., Downard, A. J., Dunne, E. M., Flagan, R. C., Kajos, M., Keskinen, H., Kirkby, J., Kupc, A., Kürten, A., Kurtén, T., Laaksonen, A., Mathot, S., Onnela, A., Praplan, A. P., Rondo, L., Santos, F. D., Schallhart, S., Schnitzhofer, R., Sipilä, M., Tomé, A., Tsagkogeorgas, G., Vehkamäki, H., Wimmer, D., Baltensperger, U., Carslaw, K. S., Curtius, J., Hansel, A., Petäjä, T., Kulmala, M., Donahue, N. M. and Worsnop, D. R.: Molecular understanding of atmospheric particle formation from sulphuric acid and large oxidized organic molecules., Proc. Natl. Acad. Sci. U. S. A., 110(43), 17223–17228, doi:10.1073/pnas.1306973110, 2013.

Simon, M., Heinritzi, M., Herzog, S., Leiminger, M., Bianchi, F., Praplan, A., Dommen, J., Curtius, J. and Kurten, A.: Detection of dimethylamine in the low pptv range using nitrate chemical ionization atmospheric pressure interface time-of-flight (CI-APi-TOF) mass spectrometry, Atmos. Meas. Tech., 9(5), 2135–2145, doi:10.5194/amt-9-2135-2016, 2016.

Sipilä, M., Sarnela, N., Jokinen, T., Henschel, H., Junninen, H., Kontkanen, J., Richters, S., Kangasluoma, J., Franchin, A., Peräkylä, O., Rissanen, M. P., Ehn, M., Vehkamäki, H., Kurten, T., Berndt, T., Petäjä, T., Worsnop, D., Ceburnis, D., Kerminen, V. M., Kulmala, M. and O'Dowd, C.: Molecular-scale evidence of aerosol particle formation via sequential addition of HIO3, Nature, 537(7621), 532–534, doi:10.1038/nature19314, 2016.

Stolzenburg, D., Fischer, L., Vogel, A. L., Heinritzi, M., Schervish, M., Simon, M., Wagner, A. C., Dada, L., Ahonen, L. R., Amorim, A., Baccarini, A., Bauer, P. S., Baumgartner, B., Bergen, A., Bianchi, F., Breitenlechner, M., Brilke, S., Buenrostro Mazon, S., Chen, D., Dias, A., Draper, D. C., Duplissy, J., El Haddad, I., Finkenzeller, H., Frege, C., Fuchs, C., Garmash, O., Gordon, H., He, X.,

https://doi.org/10.5194/acp-2020-84
Preprint. Discussion started: 4 March 2020
© Author(s) 2020. CC BY 4.0 License.

Atmospheric Chemistry and Physics Discussions

Helm, J., Hofbauer, V., Hoyle, C. R., Kim, C., Kirkby, J., Kontkanen, J., Kürten, A., Lampilahti, J., Lawler, M., Lehtipalo, K., Leiminger, M., Mai, H., Mathot, S., Mentler, B., Molteni, U., Nie, W., Nieminen, T., Nowak, J. B., Ojdanic, A., Onnela, A., Passananti, M., Petäjä, T., Quéléver, L. L. J., Rissanen, M. P., Sarnela, N., Schallhart, S., Tauber, C., Tomé, A., Wagner, R., Wang, M., Weitz, L., Wimmer, D., Xiao, M., Yan, C., Ye, P., Zha, Q., Baltensperger, U., Curtius, J., Dommen, J., Flagan, R. C., Kulmala, M., Smith, J. N., Worsnop, D. R., Hansel, A., Donahue, N. M. and Winkler, P. M.: Rapid growth of organic aerosol nanoparticles over a wide tropospheric temperature range, Proc. Natl. Acad. Sci., 201807604 [online] Available from: http://www.pnas.org/lookup/doi/10.1073/pnas.1807604115, 2018.

Tröstl, J., Chuang, W. K., Gordon, H., Heinritzi, M., Yan, C., Molteni, U., Ahlm, L., Frege, C., Bianchi, F., Wagner, R., Simon, M., Lehtipalo, K., Williamson, C., Craven, J. S., Duplissy, J., Adamov, A., Almeida, J., Bernhammer, A. K., Breitenlechner, M., Brilke, S., Dias, A., Ehrhart, S., Flagan, R. C., Franchin, A., Fuchs, C., Guida, R., Gysel, M., Hansel, A., Hoyle, C. R., Jokinen, T., Junninen, H., Kangasluoma, J., Keskinen, H., Kim, J., Krapf, M., Kürten, A., Laaksonen, A., Lawler, M., Leiminger, M., Mathot, S., Möhler, O., Nieminen, T., Onnela, A., Petäjä, T., Piel, F. M., Miettinen, P., Rissanen, M. P., Rondo, L., Sarnela, N., Schobesberger, S., Sengupta, K., Sipilä, M., Smith, J. N., Steiner, G., Tomè, A., Virtanen, A., Wagner, A. C., Weingartner, E., Wimmer, D., Winkler, P. M., Ye, P., Carslaw, K. S., Curtius, J., Dommen, J., Kirkby, J., Kulmala, M., Riipinen, I., Worsnop, D. R., Donahue, N. M. and Baltensperger, U.: The role of low-volatility organic compounds in initial particle growth in the atmosphere, Nature, 533(7604), 527–531, doi:10.1038/nature18271, 2016.

Van Damme, M., Clarisse, L., Whitburn, S., Hadji-Lazaro, J., Hurtmans, D., Clerbaux, C. and Coheur, P. F.: Industrial and agricultural ammonia point sources exposed, Nature, 564(7734), 99–103, doi:10.1038/s41586-018-0747-1, 2018.

Wang, S., Wu, R., Berndt, T., Ehn, M. and Wang, L.: Formation of Highly Oxidized Radicals and Multifunctional Products from the Atmospheric Oxidation of Alkylbenzenes, Environ. Sci. Technol., 51(15), 8442–8449, doi:10.1021/acs.est.7b02374, 2017.

Yan, C.: The role of H2SO4-NH3 anion clusters in ion-induced aerosol nucleation mechanisms in the boreal forest, Atmos. Chem. Phys., (April), 1–20, doi:10.1029/2001JD001100, 2018.

Yan, C., Nie, W., Äijälä, M., Rissanen, M. P., Canagaratna, M. R., Massoli, P., Junninen, H., Jokinen, T., Sarnela, N., Häme, S. A. K., Schobesberger, S., Canonaco, F., Yao, L., Prévôt, A. S. H., Petäjä, T., Kulmala, M., Sipilä, M., Worsnop, D. R. and Ehn, M.: Source characterization of highly oxidized multifunctional compounds in a boreal forest environment using positive matrix factorization, Atmos. Chem. Phys., 16(19), 12715–12731, doi:10.5194/acp-16-12715-2016, 2016.

Yao, L., Garmash, O., Bianchi, F., Zheng, J., Yan, C., Kontkanen, J., Junninen, H., Mazon, S. B., Ehn, M., Paasonen, P., Sipilä, M., Wang, M., Wang, X., Xiao, S., Chen, H., Lu, Y., Zhang, B., Wang, D., Fu, Q., Geng, F., Li, L., Wang, H., Qiao, L., Yang, X., Chen, J., Kerminen, V. M., Petäjä, T., Worsnop, D. R., Kulmala, M. and Wang, L.: Atmospheric new particle formation from sulphuric acid and amines in a Chinese megacity, Science (80-.)., 361(6399), 278–281, doi:10.1126/science.aao4839, 2018.

Yu, H., Zhou, L., Dai, L., Shen, W., Dai, W., Zheng, J., Ma, Y. and Chen, M.: Nucleation and growth of sub-3 nm particles in the polluted urban atmosphere of a megacity in China, Atmos. Chem. Phys., 16(4), 2641–2657, doi:10.5194/acp-16-2641-2016, 2016.

Zhang, R., Khalizov, A., Wang, L., Hu, M. and Xu, W.: Nucleation and growth of nanoparticles in

https://doi.org/10.5194/acp-2020-84
Preprint. Discussion started: 4 March 2020
© Author(s) 2020. CC BY 4.0 License.

Atmospheric Chemistry and Physics Discussions

the atmosphere, Chem. Rev., 112(3), 1957–2011, doi:10.1021/cr2001756, 2012.

Zhao, J., Eisele, F. L., Titcombe, M., Kuang, C. and McMurry, P. H.: Chemical ionization mass spectrometric measurements of atmospheric neutral clusters using the cluster-CIMS, J. Geophys. Res., 115(D8), 1–19, doi:10.1029/2009jd012606, 2010.

https://doi.org/10.5194/acp-2020-84
Preprint. Discussion started: 4 March 2020
© Author(s) 2020. CC BY 4.0 License.

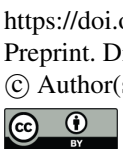

Atmospheric Chemistry and Physics Discussions

904

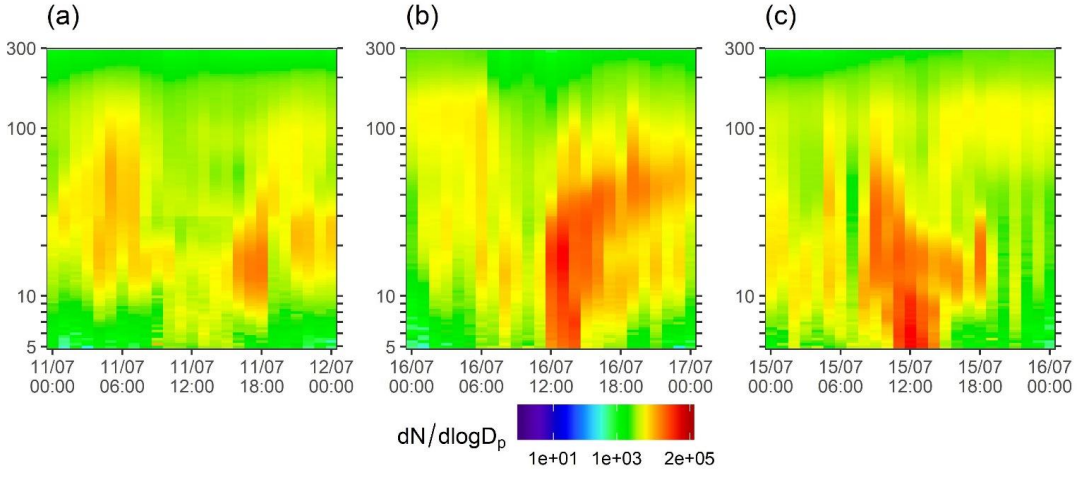

905
906

907 **Figure 1:** Example SMPS contour plots of (a) non-event day, (b) full-event day and (c) burst-event
908 day.

909

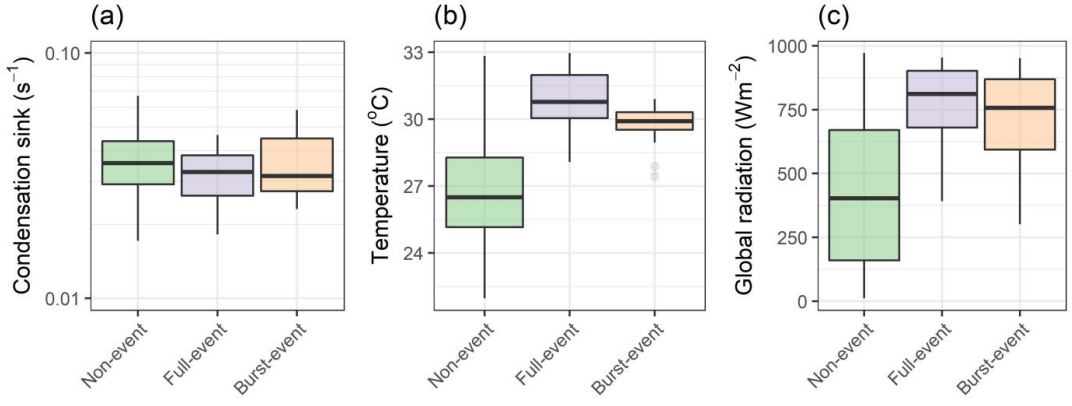

910

911 **Figure 2:** Box plots for days of non-event, full-event and burst-event, showing (a) condensation sink,
912 (b) temperature, and (c) global radiation.

913

https://doi.org/10.5194/acp-2020-84
Preprint. Discussion started: 4 March 2020
© Author(s) 2020. CC BY 4.0 License.

Atmospheric Chemistry and Physics Discussions

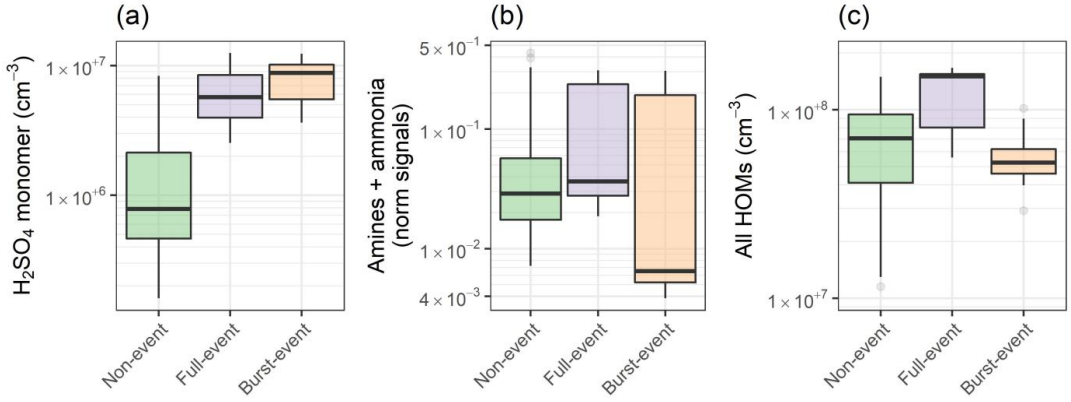

914

915 **Figure 3:** Box plots for days of non-event, full-event and burst-event, showing (a) sulphuric acid, (b)
916 ammonia, C_2 and C_4 amines, as clustered with the nitrate dimer and trimer, and (c) summed HOM
917 concentration from C_5+. Units for ammonia + amines are normalised counts, as no calibration was
918 performed.

919

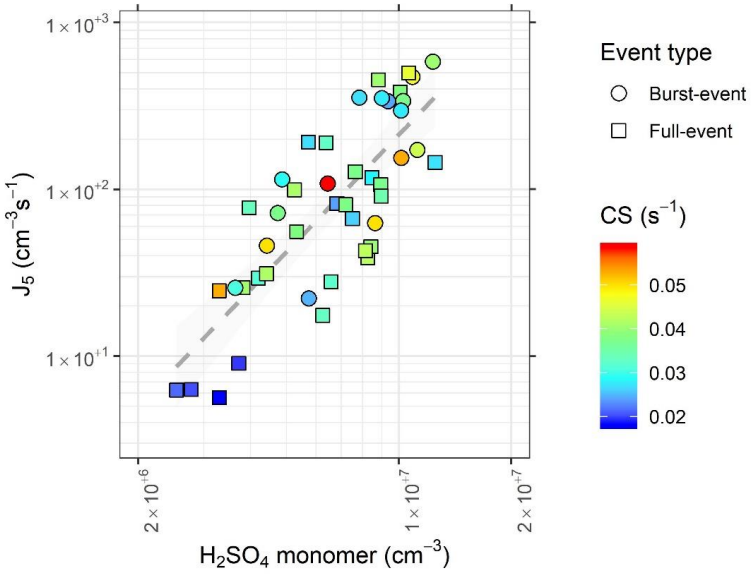

920

921 **Figure 4:** Formation rate (J_5) plotted against sulphuric acid monomer concentration, coloured by
922 condensation sink. Circles represent burst-events, squares represent full events.

https://doi.org/10.5194/acp-2020-84
Preprint. Discussion started: 4 March 2020
© Author(s) 2020. CC BY 4.0 License.

Atmospheric Chemistry and Physics Discussions

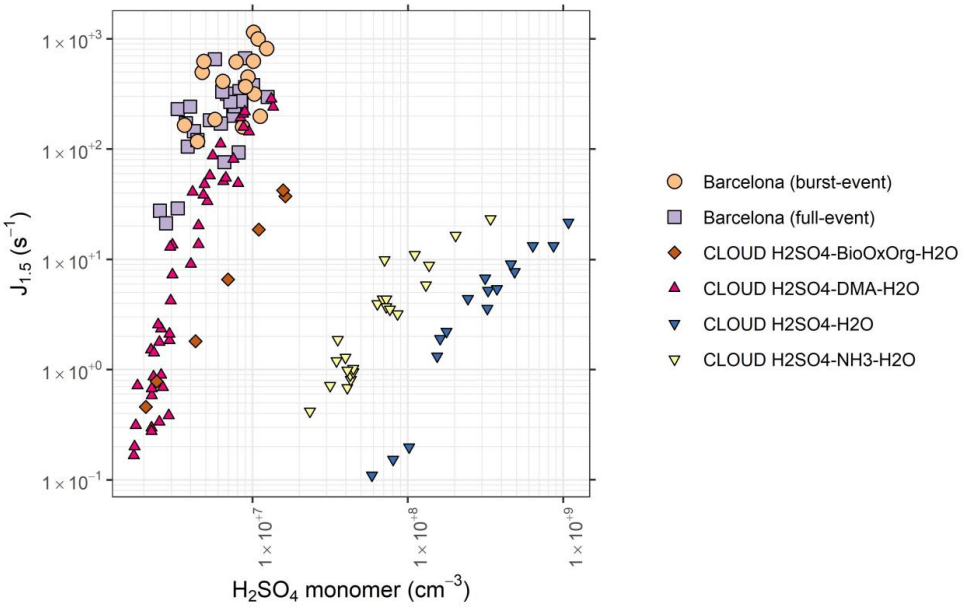

Figure 5: Formation rate ($J_{1.5}$) plotted against sulphuric acid monomer concentration for data collected from Barcelona. Tan circles represent burst-events, purple squares represent full events. as well as that for the H_2SO_4-H_2O (blue inverted triangles), H_2SO_4-NH_3-H_2O (yellow inverted triangles), H_2SO_4-DMA-H_2O (pink triangles), and H_2SO_4-BioOxOrg-H_2O (brown diamonds) systems from the CLOUD chamber (Almeida et al., 2013; Kirkby et al., 2011; Riccobono et al., 2014).

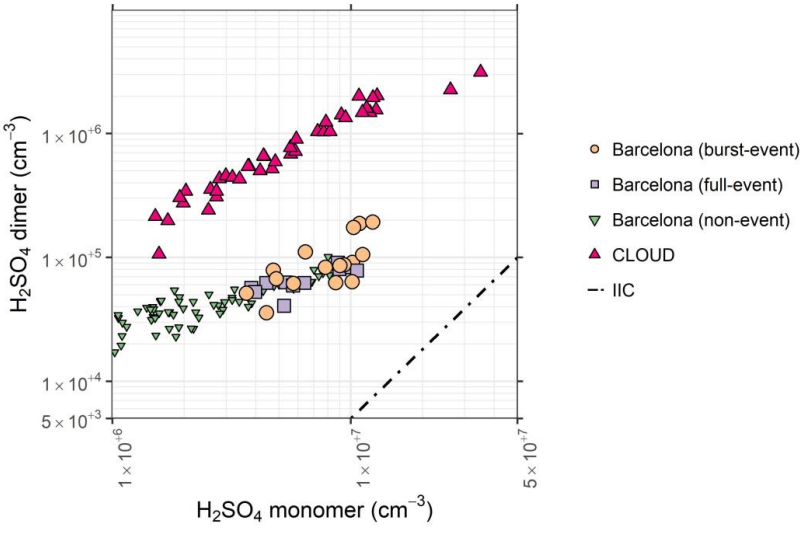

Figure 6: Sulphuric acid dimer concentration plotted against monomer concentration, showing burst-event periods (tan circles), full event periods (purple squares), non-event periods (green inverted triangles), and the ratio of sulphuric acid dimer:monomer in the CLOUD chamber for the H_2SO_4-H_2O-DMA system (pink triangles) (Almeida et al., 2013). Dashed line represents the lower limit of

https://doi.org/10.5194/acp-2020-84
Preprint. Discussion started: 4 March 2020
© Author(s) 2020. CC BY 4.0 License.

Atmospheric Chemistry and Physics Discussions

934 dimer concentration produced by ion induced clustering in the chemical ionization unit (Zhao et al.,
935 2010).

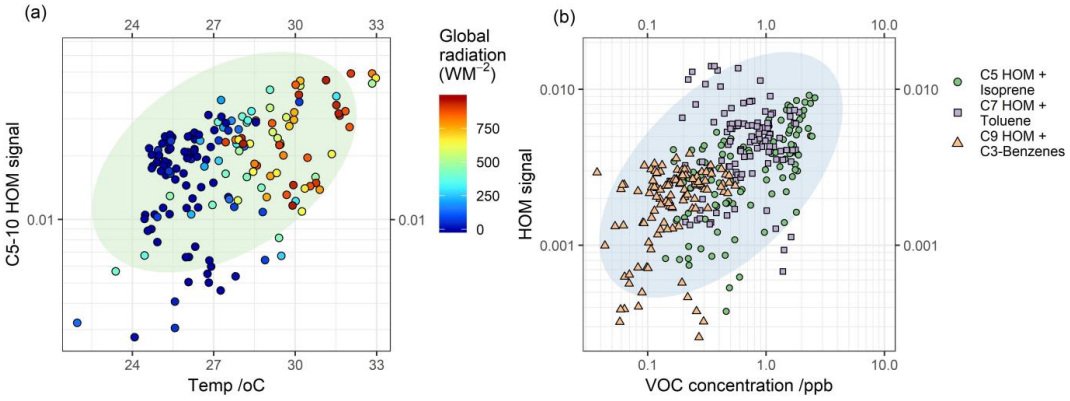

936

937 **Figure 7:** Influencing factors on VOC concentration, showing (A) temperature plotted against $C_{5\text{-}10}$
938 HOM signal, coloured by global radiation, and (B) VOC concentration plotted against HOM signal.
939 These are segregated by carbon number/VOC, i.e, C_7 HOMs plotted against toluene, under the
940 assumption that toluene oxidation is the main producer of C_7 HOMs. Ellipses show 95% confidence
941 on a multivariate t-distribution.

942

https://doi.org/10.5194/acp-2020-84
Preprint. Discussion started: 4 March 2020
© Author(s) 2020. CC BY 4.0 License.

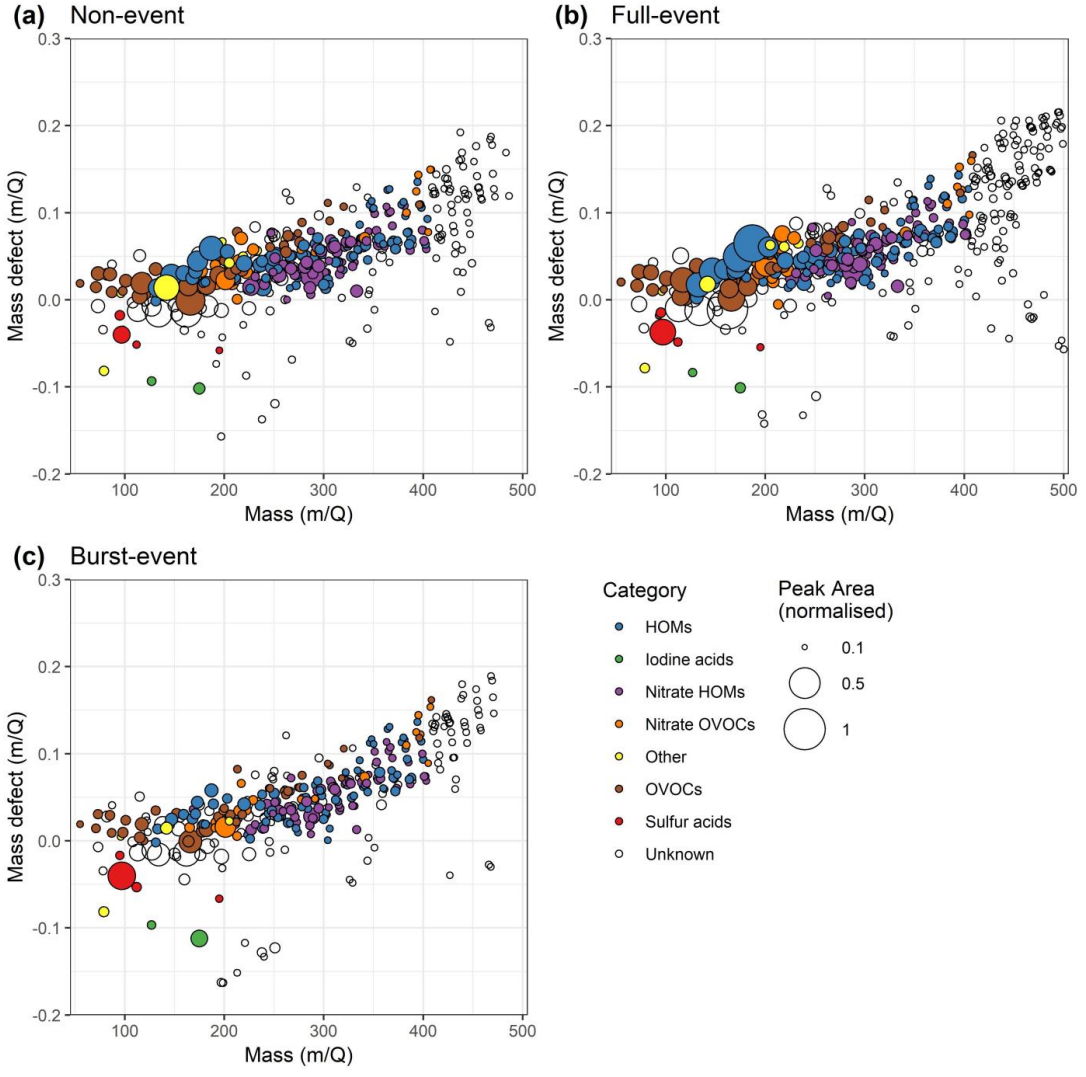

Figure 8: Mass defect plots for (a) non-event, (b) full-event, and (c) burst-event periods, data taken from 10:00 – 15:00 on the days 12/07/2018, 16/07/2018 and 15/07/2018 respectively. Size corresponds to mass spectral peak area. Ions are coloured according to identified chemical composition. *Blue* points correspond to HOMs containing all organic species with ≥5 carbon atoms and ≥6 oxygen atoms, and an O:C ratio of >0.6. *Purple* points correspond to the same but for species containing 1-2 nitrogen atoms. Species not meeting this HOM criterea were classed generally as OVOCs which are coloured *brown*, with the nitrogen containing OVOCs coloured *orange*. Sulphur acids (*red*) include ions HSO_4^-, $CH_3SO_3^-$ and SO_5^-, as well as the sulphuric acid dimer. Iodine acids (*green*) contains both IO_3^- and I^- (the latter presumably deprotonated hydrogen iodide). Unidentified points are left uncoloured.